

Brillouin spectroscopy of acoustic modes in porous silicon films

H. J. Fan,¹ M. H. Kuok,¹ S. C. Ng,¹ R. Boukherroub,^{2,*} J.-M. Baribeau,³ J. W. Fraser,³ and D. J. Lockwood³

¹Department of Physics, National University of Singapore, Singapore 117542, Republic of Singapore

²Steacie Institute for Molecular Sciences, National Research Council, Ottawa, Canada K1A 0R6

³Institute for Microstructural Sciences, National Research Council, Ottawa, Canada K1A 0R6

(Received 26 September 2001; revised manuscript received 14 February 2002; published 10 April 2002)

A systematic Brillouin study has been carried out on acoustic modes in porous silicon films prepared from *p*-type Si(100). A surface Rayleigh mode and two bulk acoustic modes, transverse and longitudinal, were observed. Results are presented for the dependence of the phase velocities of these three modes on sample porosity and film thickness. The phonon velocities, especially those of the bulk modes, increase sharply with decreasing film thickness below $\sim 10 \mu\text{m}$. This thickness dependence is attributed to the presence of a transition layer between the porous silicon film and crystalline Si substrate. Its influence on the film bulk modes increases with decreasing thickness. Elastic constants and Young's modulus of porous Si are estimated for different porosities from the phase velocities of the two bulk acoustic modes and are compared with the corresponding data obtained by other techniques.

DOI: 10.1103/PhysRevB.65.165330

PACS number(s): 78.35.+c, 68.60.Bs, 68.35.Gy, 78.55.Mb

I. INTRODUCTION

Electrochemically formed porous silicon (*p*-Si), because of its light-emitting properties and potential applications in silicon-based optoelectronic devices and in bio-chemical and chemical sensing, has drawn much research interest.¹⁻⁴ It is an unusual material whose open framework of interconnected microcrystallites varies considerably in form depending on the preparation conditions. With a suitable choice of the anodizing parameters (etchant and current density) and silicon wafer (doping and orientation), the porosity can be varied over a wide range.¹ Generally, *p*-type *p*-Si contains small pore diameters and interpore spacings, typically between 1 and 5 nm, with a highly interconnected and homogeneous pore network.¹

The surface of freshly prepared *p*-Si is covered with silicon hydrogen (Si-H_x) bonds. This termination offers good electronic properties to the material, but is subject to easy oxidation in air. Surface passivation and photoluminescence (PL) stabilization of *p*-Si were achieved by various strategies.⁵ Recently, an organic modification of the *p*-Si surfaces was successfully used for such a purpose.⁶ We have shown that the thermal reaction of hydrogen-terminated *p*-Si surfaces with alkenes and aldehydes gives organic monolayers attached through Si-C and Si-O-C bonds, respectively. These monolayers preserve the PL of the *p*-Si nanostructures and offer a high stability to the surface against oxidation.⁷⁻⁹

From an acoustic point of view, *p*-Si also has many other interesting physical properties due to its columnar or sponge-like structure. As the pore diameters are much smaller than the typical acoustic phonon wavelength of $\sim 300 \text{ nm}$, acoustic waves are expected on top of and within *p*-Si films. It would therefore be interesting to study the effect of structural variance on the elastic properties of *p*-Si compared to crystalline Si (*c*-Si). Investigations into the elastic and acoustic properties of *p*-Si were made using acoustic techniques,¹⁰ nanoindentation¹¹ and Brillouin spectroscopy.¹²⁻¹⁴ In particular, the existence of surface- and film-guided acoustic waves in these films was reported in Brillouin light scattering

studies. Andrews *et al.* investigated the surface acoustic waves in low porosity (30%) *p*-Si, and observed the Rayleigh mode.¹² In their study of surface and bulk acoustic phonons in low and high porosity *p*-Si, Beghi *et al.*¹³ found three surface acoustic phonons in their high porosity samples whose velocities exhibited dispersion. The Brillouin spectrum of 80% porosity *p*-Si, recorded by Lockwood *et al.*,¹⁴ revealed two well-separated broad peaks at about 8 and 14 GHz, assigned as the Rayleigh mode and longitudinal guided mode, respectively.

We have carried out a systematic Brillouin study of acoustic modes in H-terminated and 1-decene-passivated *p*-Si films of different thicknesses (1–26 μm) and porosities (57–83%). In general, we find that films of *p*-Si on Si(100) can sustain three kinds of acoustic waves, viz. the Rayleigh mode, a bulk transverse acoustic (TA) mode, and a longitudinal acoustic (LA) mode. The two bulk acoustic modes are analyzed with regard to their porosity dependence and the corresponding elastic parameters are extracted from the Brillouin data. Some of our results are significantly different from those of previous Brillouin studies of *p*-Si.¹²⁻¹⁴

II. EXPERIMENTAL METHOD

The *p*-Si samples used in this study were prepared by anodizing B-doped, single-side polished (100) *p*-type silicon wafers. The silicon wafers were first cleaned in 3:1 concentrated H₂SO₄/30% H₂O₂ for 5 min at room temperature, and then rinsed copiously with Milli-Q water. The clean wafers were immersed in 48% aqueous HF solution for 1 min at room temperature to remove the native oxide. The samples were then electrochemically anodized in 48% aqueous HF and ethanol solution at current densities of 2–40 mA/cm² and an etching period of 8 or 80 min to achieve 57–83% porosity and 2.2–26- μm film thickness. Details of the preparation conditions for H-terminated samples used in the porosity study are given in Table I. After etching, the samples were rinsed with pure ethanol and dried under a stream of dry nitrogen. For the thickness study, samples were prepared

TABLE I. Preparation conditions, porosity, and thickness of H-terminated *p*-Si films prepared from *p*-type Si (100) wafers.

Sample	Si wafer resistivity Ω cm	HF/EtOH (v/v)	Current density (mA cm ⁻²)	Etching time (min)	Porosity (%)	Thickness (μ m)
1	1.0–1.05	1:1	5	8	70	3.06
2	1.48–1.84	1:1	10	8	72	6.24
3	1.48–1.84	1:1	30	8	75	12.0
4	1.0–1.05	1:1	30	8	77	5.03
5	1.0–1.05	1:1	40	8	79	20.6
6	0.005	1:1	20	8	60	10.36
7	0.005	1:1	40	8	63	20.3
8	1.48–1.84	1:3	5	8	83	2.17
9	1.48–1.84	1:3	10	8	83	5.04
10	1.48–1.84	1:1	5	8	70	2.77
11	1.48–1.84	1:1	5	8	70	2.95
12	1.48–1.84	1:1	5	8	70	3.04
13	1.48–1.84	1:1	2	80	79	9.45
14	1.0–1.05	1:1	5	8	74	3.0
15	1.0–1.05	1:1	5	8	78	2.82
16	0.005	3:1	40	8	57	26.0

from 1.48–1.84- Ω cm silicon wafers in a 1:1 etching solution of HF:EtOH at a current density of 5 mA/cm² to produce a porosity of 70%. Etching times of 4, 8, 16, 32, and 64 min were used to vary the film thickness from \sim 1 to 24 μ m. The H-terminated surfaces of these freshly prepared *p*-Si samples were chemically modified with 1-decene at 115 °C (Refs. 7–9) to form *p*-Si passivated with C₁₀H₂₁ (abbreviated to C-passivated *p*-Si). The passivation process is active throughout the entire depth of the *p*-Si layer (confirmed by Auger spectroscopy) and protects the pore surfaces against oxidation in ambient air.^{7–9}

Sample porosities were determined by low-angle x-ray reflectivity.¹⁵ The specular reflectivity from the sample was measured using a Philips MRD diffractometer equipped with a four-crystal monochromator (220 reflections) and a 0.1-mm receiving slit. The index of refraction of a solid surface at x-ray wavelengths is slightly less than unity, and results in total reflection of x rays up to a critical angle typically of a few tenths of a degree. In the reflectivity curve, the critical angle (ϕ_{p-Si} for *p*-Si and ϕ_{c-Si} for *c*-Si) corresponds to the angle at which the reflectivity starts to decrease sharply, due to an increased penetration of x rays through the solid. The critical angle is proportional to the square root of the electronic density, and its measurement provides an easy and accurate means of determining the density at the surface of impurity-free elemental materials or stoichiometric compounds. A typical x-ray reflectivity curve is shown in Fig. 1. The porosities (ϵ) of the freshly prepared H-terminated samples listed in Table I were calculated from¹⁵ $\epsilon = 1 - (\phi_{p-Si}/\phi_{c-Si})^2$.

Scanning electron microscopy (SEM) images were obtained with a Field Emission Hitachi S4700 using an accelerating voltage of 5.0 keV. The SEM measurements were used to study the pore morphology and to determine the *p*-Si film thickness given in Table I. The very dense and vertical

cylindrical pore channels are clearly visible in the typical plan view and cross sectional SEM images shown in Fig. 2. The *p*-Si nanocrystallite size was found using Raman scattering, which was performed at room temperature in a quasi-backscattering geometry using 30 mW of 457.9-nm laser excitation. A typical Raman spectrum is shown in Fig. 3. From the shift in frequency relative to the *c*-Si Raman peak, the nanocrystallite sizes of the samples studied were estimated¹⁶ to range from 4 to 10 nm. Raman spectroscopy confirmed the presence of H in the freshly prepared *p*-Si samples through the observation of characteristic SiH_x peaks (see Fig. 3).

Brillouin spectra were recorded in the 180°-backscattering geometry using a (3+3)-pass tandem Fabry-Pérot interferometer. The free spectral range was set between 12.5 and 50.0 GHz. A laser light of 514.5 nm wavelength was used with the incident beam power kept below 25 mW to prevent sample damage. All measurements were carried out at room

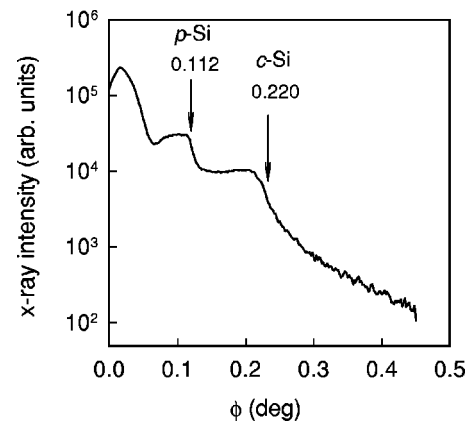


FIG. 1. X-ray reflectivity spectrum of H-terminated *p*-Si. The porosity is calculated (Ref. 15) to be $\epsilon = 1 - (0.112/0.220)^2 \approx 74\%$.

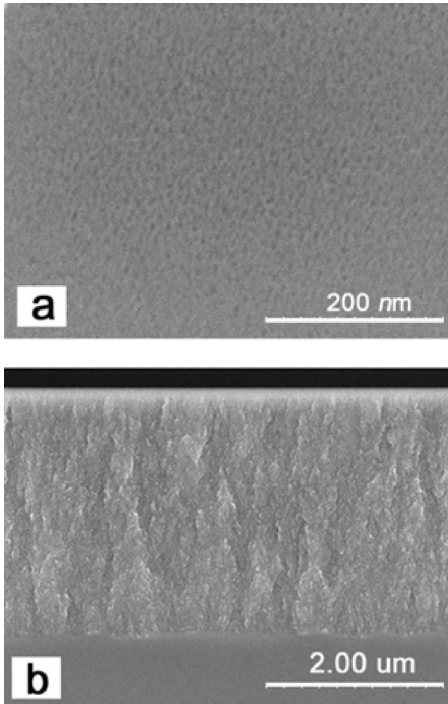


FIG. 2. (a) Plan view and (b) cross-sectional SEM images of a 78% porosity, 2.82- μm -thick H-terminated p -Si film prepared from p -type Si(100).

temperature. A stream of pure, dry argon gas was directed at the irradiated spot on the sample to cool it and to keep air away from it. The refractive index of our p -Si is estimated to be about 1.5,¹⁷ much lower than that of crystalline silicon (≈ 4.2). Thus, for the excitation wavelength used in this study, the p -Si films are effectively optically transparent. The incident light wave vector \mathbf{k}_0 made an angle θ with respect to the (100) surface normal, and the backscattered light is collected from within the solid angle around $-\mathbf{k}_0$. Spectra were recorded in p - p and p - s polarization configurations, typically for a duration of one hour.

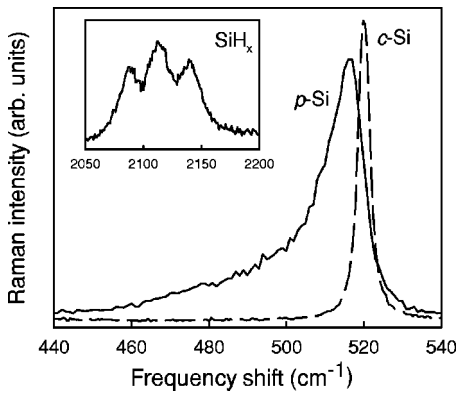


FIG. 3. Raman spectrum of 70% porosity, 2.0- μm -thick H-terminated p -Si (continuous line) and of c -Si (dash line). The frequency shift from 520 cm^{-1} in c -Si to 516 cm^{-1} in p -Si indicates an average spherite diameter of 5 nm (Ref. 16). The inset shows Raman peaks at 2089, 2113, and 2139 cm^{-1} due to SiH_x .

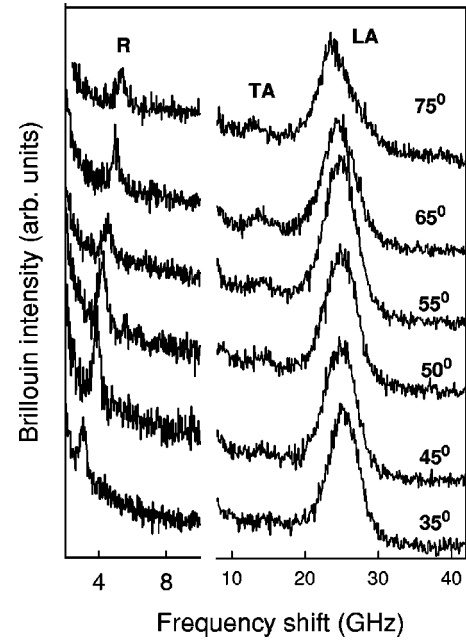


FIG. 4. Brillouin spectra of 70% porosity, 3.0- μm -thick H-terminated p -Si obtained at various angles of incidence. R: Rayleigh mode; TA: bulk transverse acoustic mode; LA: bulk longitudinal acoustic mode.

III. RESULTS AND DISCUSSION

A. Spectra and assignment of modes

Figure 4 shows the Brillouin spectra of a 70% porosity, 3.0- μm -thick H-terminated p -Si sample recorded at various angles of incidence θ in p - p polarization. (The p - s -polarized spectra were found to be featureless.) In general, the spectrum features three peaks centered at about 4, 14, and 25 GHz, which are respectively assigned (see below) to the surface Rayleigh mode, a bulk TA mode, and a bulk LA mode.

Figure 5 shows the thickness dependence of the Brillouin spectrum of 70%-porosity C-passivated p -Si for one angle of incidence. It is clear that with increasing film thickness all the peaks shift to lower frequencies. Similar results were obtained for other values of θ . It is noteworthy that the highest-frequency peak appears as a doublet for some samples. This feature is ascribed to a relatively abrupt change in porosity inhomogeneity across the sample depth, as evidenced by cross sectional SEM images.

The phase velocities of the Rayleigh mode (v_R) and bulk modes (v_B) were computed from their Brillouin frequencies (ν_R and ν_B) using

$$v_R = \lambda \nu_R / (2 \sin \theta),$$

$$v_B = \lambda \nu_B / (2n) \quad (1)$$

where λ is the excitation wavelength. The refractive index of p -Si, n , is calculated from the empirical formula for porosity ϵ ,¹⁷

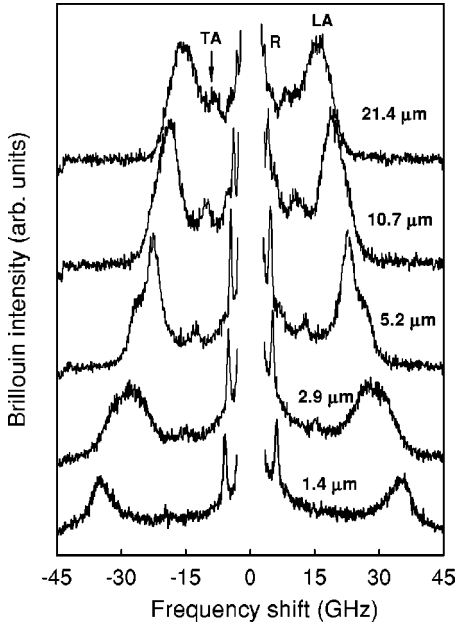


FIG. 5. Brillouin spectra of 70% porosity C-passivated *p*-Si of various film thicknesses. The angle of incidence is 60°. R: Rayleigh mode; TA: bulk transverse acoustic mode; LA: bulk longitudinal acoustic mode. For some spectra, a doublet LA is observed (see the discussion in the text).

$$1 - \epsilon = \frac{(1 - n^2)(N^2 + 2n^2)}{3n^2(1 - N^2)}, \quad (2)$$

where $N=4.22$ is the refractive index of *c*-Si at the wavelength of 514.5 nm. The phonon velocities of the three modes in 70% porosity C-passivated *p*-Si for two film thicknesses are shown in Fig. 6 as a function of θ . Results obtained for H-terminated *p*-Si and for other porosities and film thicknesses are qualitatively similar. As can be seen in Fig. 6,

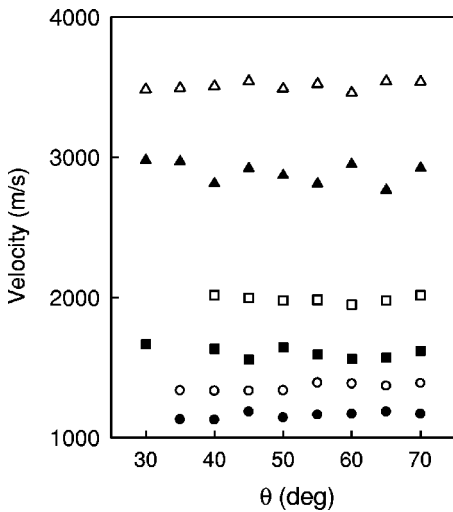


FIG. 6. Phase velocities of the Rayleigh (circle), TA (square), and LA (triangle) vs the angle of incidence for 70% porosity C-passivated *p*-Si films. Open symbols: 5.24 μm thick; filled symbols: 10.7 μm thick.

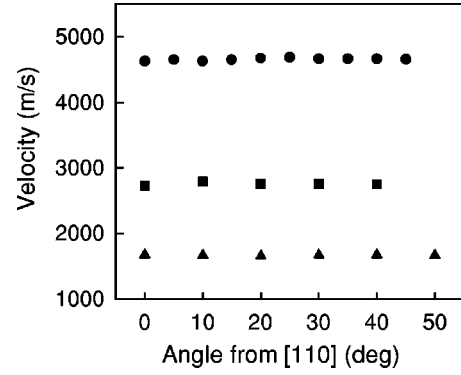


FIG. 7. Acoustic mode velocities of *p*-Si films vs their propagating directions relative to the [110] direction of the Si substrate. Triangle: Rayleigh velocity of 70% porosity, 1.1 μm thick C-passivated *p*-Si. Square: Rayleigh velocity of 57% porosity, 26.0 μm thick H-terminated *p*-Si. Circle: LA mode velocity of 70% porosity, 2.8 μm thick H-terminated *p*-Si.

all three modes show no obvious velocity dispersion with increasing θ , within experimental error.

The very sharp lowest-frequency peak, below 10 GHz, was assigned to scattering from the surface Rayleigh mode. Its frequency is proportional to $\sin \theta$, which is characteristic of real surface modes. Thus it is not surprising that it does not exhibit any velocity dispersion (see Fig. 6). This sharp mode was not observed in our earlier study¹⁴ based on a single thick (25 μm) *p*-Si slab sample, and thus was incorrectly identified in that study. The Rayleigh peak in the present study has an extremely small linewidth (≈ 0.2 GHz), in contrast to those of *p*-Si films (≈ 2 GHz) measured by Beghi *et al.*¹³ and of cluster-assembled carbon films measured by Bottani *et al.*,¹⁸ in which cases the broadened phonon peaks and the presence of an intense elastic background probably arise from sample surface roughness and inhomogeneity. This suggests that our *p*-Si samples have good surface quality on a mesoscopic length scale, as borne out by SEM data. Unlike the conclusion drawn by Andrews *et al.* in their Brillouin study of 30% porosity (111)-oriented *p*-Si,¹² our Rayleigh mode velocity is independent of its propagating direction, as shown in Fig. 7, and thus our higher porosity *p*-Si surfaces [originally Si (100)] are elastically isotropic.

The intermediate-frequency peak is weak as well as broad, and arises from a mode whose velocity is independent of incident angles. Empirically, the frequency of this peak is too high, relative to the Rayleigh wave, to be that of a Sezawa wave, which is a film mode propagating parallel to the film surface. In addition, Rowell *et al.*¹⁹ established that the number of orders of Sezawa waves, in supported films, increases with increasing film thickness. However, no additional peaks were observed in the vicinity of the intermediate-frequency peak for the thicker films. Neither can it be a Stoneley wave, which is an interface mode, for the reason that the transverse acoustic velocity in *p*-Si is much smaller than that in the *c*-Si substrate (also see below). This peak is instead assigned to a bulk TA mode in *p*-Si. In our spectra, the TA peak is observable only for some samples and for incidence angle θ larger than 50° (see Fig. 4). Although,

in an elastically isotropic medium, Brillouin scattering from the TA mode is theoretically forbidden in an exact 180° backscattering configuration,²⁰ it was most probably detected because of the finite aperture ($f/2$) of the lens collecting the scattered light.

The highest-frequency peak is also associated with a bulk mode, primarily because its frequency is insensitive to θ . This mode cannot be a longitudinal guided mode localized inside the film, because its frequency is more than five times that of the Rayleigh mode (see Fig. 4), and hence too high.²¹ Moreover, it still appears as a dominant peak in spectra of p -Si films that are up to $20\ \mu\text{m}$ thick, whereas a longitudinal guided mode tends to be unobservable at large film thicknesses ($>3\ \mu\text{m}$) due to the breakdown of the resonance condition.²¹ Therefore, the highest-frequency peak is ascribed to the bulk LA mode of the p -Si film. Except for the bulk LA mode ($\approx 140\ \text{GHz}$) of the c -Si (100) substrate, no other acoustic mode was observed at higher frequencies for the p -Si films. The $\sim 140\ \text{GHz}$ peak observed by Beghi *et al.*¹³ in their Brillouin spectrum of n -type p -Si of 30% porosity most probably originates from the c -Si substrate, instead of from the p -Si film.

A prominent feature of the LA peak is its large linewidth ($\sim 3\text{--}5\ \text{GHz}$) compared to that of the Rayleigh peak ($\approx 0.2\ \text{GHz}$). This indicates a considerable scattering of the phonon by interior structural irregularities, i.e., the intrinsic inhomogeneity, resulting from the anodizing process, of the crystalline Si skeleton within the depth of the p -Si film. The top surface of the p -Si film, however, retains the flatness of the original c -Si (100) wafer surface.

B. Variation of mode velocity with film thickness

For the study of film thickness effect, samples were chosen from those prepared under similar conditions but for different etching times so that similar porosities were expected. Figure 8 shows the thickness dependence of phase velocities of the Rayleigh, TA, and LA modes in the H-terminated and C-passivated p -Si samples. The figure reveals that the velocities of these three modes in C-passivated p -Si are almost the same as their corresponding ones in H-terminated p -Si. This implies that surface passivation with 1-decene has little effect on the mode velocities of p -Si. The Rayleigh mode velocity is quite independent of p -Si layer thickness at larger thicknesses. This is not surprising as the Rayleigh wave, being a true surface wave, propagates on the top surface of the film only, and its velocity should not be greatly affected by layer thickness, at least not for the thicknesses greater than $10\ \mu\text{m}$.

In contrast, the velocities of the two bulk modes are strongly influenced by the thickness. For both H-terminated and C-passivated p -Si, the bulk mode velocities increase sharply with decreasing film thickness below $\sim 10\ \mu\text{m}$. This thickness dependence can be attributed to the presence of a transition layer between the p -Si film and the c -Si substrate, within which its elastic properties vary from those of the p -Si to those of c -Si. For a large film thickness the mode velocities reflect the elastic properties of the film. However, as the film thickness decreases, the transition layer will have a

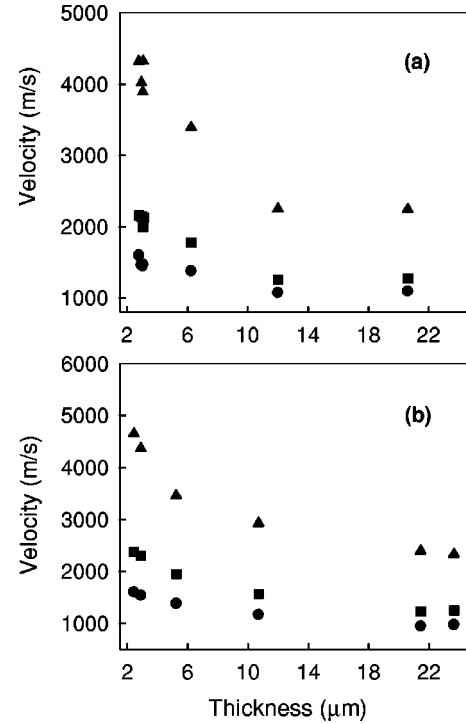


FIG. 8. Phase velocities of the three acoustic modes in 70% porosity (a) H-terminated and (b) C-passivated p -Si as a function of film thickness. Data were obtained from spectra taken at an incident angle of 60° . Circle: Rayleigh mode; square: TA mode; triangle: LA mode.

larger influence on the bulk mode velocities of the film. For sufficiently thin layers, the LA mode ($\sim 140\ \text{GHz}$) of the c -Si substrate starts to appear in the spectrum. A film thickness dependence of other physical properties was also observed in different systems: e.g., the dielectric permittivity and the effective longitudinal piezoelectric coefficient of ceramic films,^{22,23} and the photoconductivity of a amorphous carbon.²⁴

C. Variation of mode velocity with porosity

As its velocity is quite insensitive to film thickness, determining the porosity dependence of the Rayleigh wave velocity is relatively straightforward. Figure 9(a) shows our results, together with Brillouin data measured by Andrews *et al.*¹² and Beghi *et al.*¹³ as well as data determined by acoustic techniques,¹⁰ for the Rayleigh mode velocity versus porosity in H-terminated p -Si. Experimental data for zero porosity (c -Si) was obtained from Ref. 25. The dependence of the velocity on porosity is essentially linear within experimental error, which mainly arises from the determination of porosity.

In contrast, the determination of the variation of the TA and LA velocities with porosity is made difficult by their strong dependence on layer thickness (see Fig. 8). From the above discussion, only data for thick layers ($>10\ \mu\text{m}$) were used to ascertain the thick film limit of the porosity dependence of the TA and LA velocities. Results for the H-terminated and C-passivated samples are displayed in

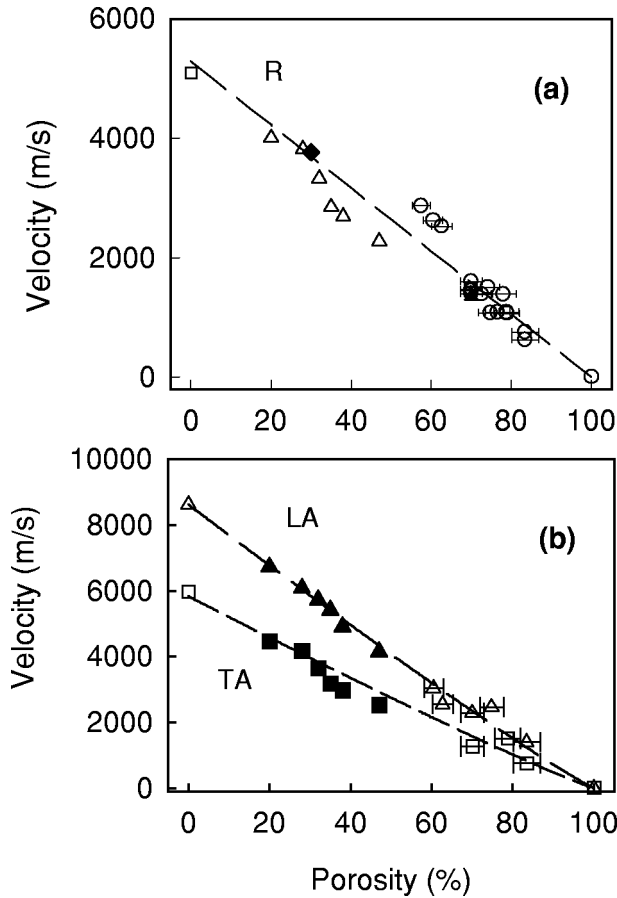


FIG. 9. Variation of acoustic mode velocities of *p*-Si with porosity. (a) The Rayleigh mode of H-terminated *p*-Si: results of present study (open circle), Andrews *et al.* (Ref. 12) (diamond), Beghi *et al.* (Ref. 13) (filled triangle), and Fonseca *et al.* (Ref. 10) (open triangle). Data from Schindel *et al.* (Ref. 25) for *c*-Si was also included (square). (b) LA mode (triangle) and TA mode (square) of H-terminated and C-passivated *p*-Si: shown are results of the present study (open symbols) and those of Fonseca *et al.* (filled symbols). The data for zero porosity are the corresponding theoretical bulk LA and TA velocities of *c*-Si in the [100] direction. Dashed lines correspond to the fits with $v = v_0(1 - \varepsilon)^m$ (see the text). The error bars for the velocities are smaller than the symbols used to represent them.

Fig. 9(b), in which the corresponding bulk velocities determined by Fonseca *et al.*¹⁰ were also included. It is seen that the data obtained by the acoustic technique are consistent with those measured by Brillouin scattering, and that an increase of porosity leads to a linear drop of the bulk mode velocities.

The relationship between the acoustic mode velocities of *c*-Si and those of *p*-Si is¹⁰

$$v = v_0(1 - \varepsilon)^m, \quad (3)$$

where v and v_0 are the surface and bulk mode velocities in *p*-Si and *c*-Si, respectively, and m is an empirical parameter depending on the microstructural details of the porous solid. Use of Eq. (3) to fit our experimental data yielded the following values of m : 1.004 (Rayleigh mode), 1.086 (TA), and

TABLE II. Acoustic mode velocities and elastic parameters for 70%-porosity H-terminated and C-passivated *p*-Si.

<i>p</i> -Si	v_{TA} (m/s)	v_{LA} (m/s)	c_{11} (GPa)	c_{12} (GPa)	E (GPa)	v_R^a (m/s)	v_R^b (m/s)
H-terminated	1250	2250	3.40	1.30	2.68	1100	1158
C-passivated	1200	2300	3.55	1.62	2.54	1000	1118

^aExperimental value of the Rayleigh velocity extrapolated from Fig. 8.

^bThe Rayleigh velocity calculated using Eq. (6).

1.083 (LA), which are all within the 0.5–1.5 range. This indicates, based on findings by Phani *et al.*,²⁶ that our samples have a relatively ordered and less-open pore structure, which is consistent with the observations made using SEM (see, for example, Fig. 2)

D. Estimation of elastic parameters

Knowledge of the bulk mode velocities allows us to deduce the elastic parameters of bulk *p*-Si material. As shown in Fig. 8, the bulk mode velocities show negative dispersion with thickness and the limiting mode velocities for *p*-Si are attained for films thicker than $\sim 20 \mu\text{m}$. For isotropic media, the relationships between elastic constants and acoustic velocities in the infinite thickness limit are

$$v_{LA} = \sqrt{c_{11}/\rho},$$

$$v_{TA} = \sqrt{(c_{11} - c_{12})/2\rho} \quad (4)$$

where ρ is the density of *p*-Si which is related to that of *c*-Si (ρ_0) by $\rho = \rho_0(1 - \varepsilon)$. Hence the elastic constants c_{11} and c_{12} can be deduced from the experimental mode velocities v_{TA} and v_{LA} , which in our case were determined for the thickest films ($\sim 20 \mu\text{m}$) as approximate values for the asymptotic velocities of the TA and LA modes, respectively, for infinitely thick films. Young's modulus E , in isotropic media, can be expressed in terms of the elastic constants as

$$E = (c_{11} + 2c_{12})(c_{11} - c_{12})/(c_{11} + c_{12}). \quad (5)$$

In addition, the surface Rayleigh mode velocity v_R can be calculated using Viktorov's relation:²⁷

$$v_R \approx v_{TA}(0.87c_{11} + 2c_{12})/(c_{11} + 2c_{12}) \quad (6)$$

Table II summarizes the results obtained in this way for samples of 70% porosity. The experimental values of the Rayleigh velocity are also presented for comparison.

The results given in Table II show that the velocities of the TA and LA modes in *p*-Si are significantly smaller than the corresponding values of ~ 5800 and ~ 8600 m/s in *c*-Si. Also note that the mode velocities are almost the same in the C-passivated film as those in the H-terminated one, indicating negligible effect from the passivation of 1-decene. Our Young's modulus values are very close to that of 2.4 GPa obtained for *p*-type *p*-Si of 70% porosity by Bellet *et al.*¹¹ using the nanoindentation technique. In addition, the calculated Rayleigh velocities are slightly higher than the experi-

mental values. This small discrepancy in the Rayleigh velocity mainly results from overestimation of c_{11} and c_{12} due to the finite thickness of the films studied.

In order to understand how the sample porosity affects the elastic constants and Young's modulus, we applied Eqs. (4) and (5) to samples of various porosities and film thicknesses ($>10 \mu\text{m}$). Sample with large film thicknesses were chosen in order to minimize the influence of film thickness in estimating the bulk velocities, as mentioned above. For comparison, the calculation was also performed for the case where the shear and longitudinal mode velocities were obtained by acoustic methods.¹⁰ The results obtained are shown in Fig. 10. It can be seen that both c_{11} and c_{12} , calculated from Brillouin data, fits in well with the general trends. This good agreement corroborates our assignment of the two higher frequency peaks to bulk TA and LA modes.

The calculated Young's modulus data from our results were fitted with¹¹

$$E = E_0(1 - \varepsilon)^l, \quad (7)$$

where E_0 is Young's modulus of c -Si and $l = 2m + 1$, where m is the empirical parameter for the LA mode in Eq. (3). The fitted values are $E_0 = 155 \text{ GPa}$ and $l = 2.93$. This value of E_0 is comparable to the measured Young's modulus of 162 GPa for c -Si.¹¹ The magnitude of l is quite consistent with the value of 1.083 obtained above for m . For comparison, data obtained using nanoindentation methods,¹¹ acoustic techniques¹⁰ and Brillouin scattering by Andrews *et al.*¹² are also included. There is, in general, good agreement between the results obtained by these various methods.

IV. CONCLUSION

This comprehensive Brillouin study of acoustic waves in p -Si films has allowed the identification of the three types of acoustic modes observed. The velocities of the three modes are found to exhibit a negative dispersion with porosity. Because of the high porosity, values for the velocities of the TA and LA modes in p -Si are much lower than those of c -Si. The surface Rayleigh mode velocity is quite independent of the incidence angle and, as expected, is least affected by the p -Si film thickness. On the other hand, the TA and LA modes exhibit negative velocity dispersion with the film thickness, i.e., as the film thickness decreases below $\sim 10 \mu\text{m}$, their velocities increase sharply. The thickness dependence is at-

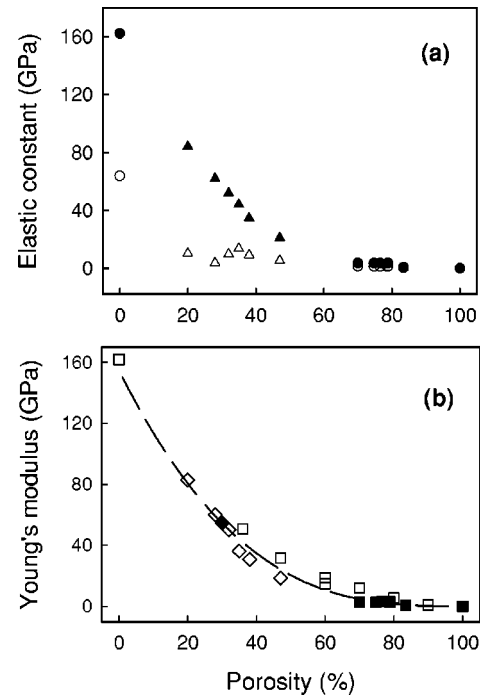


FIG. 10. Variation of elastic parameters of H-terminated p -Si with sample porosity. (a) Elastic constants: filled and open symbols represent c_{11} and c_{12} , respectively. Triangles denote acoustic data from Fonseca *et al.* (Ref. 10). Elastic constants at zero porosity correspond to those of c -Si. (b) Young's modulus: filled square, present study; open square, nanoindentation (Ref. 11); open diamond, acoustic (Ref. 10); filled diamond: Brillouin scattering (Ref. 12). The dashed line corresponds to a fit of $E = E_0(1 - \varepsilon)^l$ to our data (see the text).

tributed to the presence of a transition layer between the p -Si film and c -Si substrate. The asymptotic velocities of the bulk modes at large thicknesses have enabled us to estimate the elastic constants as well as Young's modulus of p -Si. Increasing the porosity leads to a nonlinear decrease of the elastic constants and Young's modulus.

ACKNOWLEDGMENTS

This work was supported in part by the National University of Singapore under Research Project No. R-144-000-018-112, and through the award of a scholarship to H. J. Fan.

*Current address: Physique de la Matière Condensée, Ecole Polytechnique, Route de Saclay, 91128 Palaiseau, France.

¹A.G. Cullis, L.T. Canham, and P.D.J. Calcott, *J. Appl. Phys.* **82**, 909 (1997).

²V. Parkhutik, *Solid-State Electron.* **43**, 1121 (1999).

³O. Bisi, S. Ossicini, and L. Pavesi, *Surf. Sci. Rep.* **38**, 1 (2000).

⁴M.P. Stewart and J.M. Buriak, *Adv. Mater.* **12**, 859 (2000).

⁵J.-N. Chazalviel and F. Ozanam, in *Microcrystalline and Nanocrystalline Semiconductors*, edited by M.J. Sailor, C.C. Tsai, L.T. Canham, and T. Kanaka, MRS. Conf. Proc. No. 536 (Materials Research Society, Pittsburgh, 1999), p. 155.

⁶J.M. Buriak, *Chem. Commun. (Cambridge)* **1999** (12), 1051

(1999).

⁷R. Boukherroub, S. Morin, D.D.M. Wayner, and D.J. Lockwood, *Phys. Status Solidi A* **182**, 117 (2000).

⁸R. Boukherroub, S. Morin, D.D.M. Wayner, and D.J. Lockwood, *Solid State Commun.* **118**, 319 (2001).

⁹R. Boukherroub, S. Morin, D.D.M. Wayner, F. Bensebaa, G.I. Sproule, J.-M. Baribeau, and D.J. Lockwood, *Chem. Mater.* **13**, 2002 (2001).

¹⁰R.J.M. Da Fonseca, J.M. Saurel, A. Foucaran, J. Camassel, E. Massone, T. Taliércio, and Y. Boumaiza, *J. Mater. Sci.* **30**, 35 (1995).

¹¹D. Bellet, P. Lamagnère, A. Vincent, and Y. Bréchet, *J. Appl.*

- Phys. **80**, 3772 (1996).
- ¹²G.T. Andrews, J. Zuk, H. Kiefte, M.J. Clouter, and E. Nossarzewska-Orlowska, *Appl. Phys. Lett.* **69**, 1217 (1996).
- ¹³M.G. Beghi, C.E. Bottani, G. Ghislotti, G. Amato, and L. Boarino, *Thin Solid Films* **297**, 110 (1997).
- ¹⁴D.J. Lockwood, M.H. Kuok, S.C. Ng, and Z.L. Rang, *Phys. Rev. B* **60**, 8878 (1999).
- ¹⁵D. Buttard, G. Dolino, D. Bellet, T. Baumbach, and F. Rieutord, *Solid State Commun.* **109**, 1 (1999).
- ¹⁶Z. Sui, P.P. Leong, I.P. Herman, G.S. Higashi, and H. Temkin, *Appl. Phys. Lett.* **60**, 2086 (1992).
- ¹⁷C. Pickering, M.I.J. Beale, D.J. Robbins, P.J. Pearson, and R. Greef, *J. Phys. C* **17**, 6535 (1984).
- ¹⁸C.E. Bottani, A.C. Ferrari, A.L. Bassi, P. Milani, and P. Piseri, *Europhys. Lett.* **42**, 431 (1998).
- ¹⁹N.L. Rowell and G.I. Stegeman, *Phys. Rev. Lett.* **41**, 970 (1978).
- ²⁰J. R. Sandercock, in *Light Scattering in Solids III*, edited by M. Cardona and G. Güntherodt, *Topics in Applied Physics Vol. 51* (Springer-Verlag, Berlin, 1982), p. 173.
- ²¹B. Hillebrands, S. Lee, G.I. Stegeman, H. Cheng, J.E. Potts, and F. Nizzoli, *Phys. Rev. Lett.* **60**, 832 (1988).
- ²²H.D. Chen, K.R. Udayakumar, C.J. Gaskey, L.E. Cross, J.J. Bernstein, and L.C. Niles, *J. Am. Ceram. Soc.* **79**, 2189 (1996).
- ²³K.R. Udayakumar, P.J. Schuele, J. Chen, S.B. Krupanidhi, and L.E. Cross, *J. Appl. Phys.* **77**, 3981 (1995).
- ²⁴D.R. McKenzie, Y. Yin, N.A. Marks, C.A. Davis, E. Kravtchinskaia, B.A. Pailthorpe, and G.A.J. Amaratunga, *J. Non-Cryst. Solids* **164-166**, 1101 (1993).
- ²⁵D.W. Schindel, D.A. Hutchins, S.T. Smith, and B. Farahbakhsh, *J. Acoust. Soc. Am.* **95**, 2517 (1994).
- ²⁶K.K. Phani, S.K. Niyogi, A.K. Maitra, and M. Roychaudhury, *J. Mater. Sci.* **21**, 4335 (1986).
- ²⁷I. A. Viktorov, *Rayleigh and Lamb Waves: Theory and Applications* (Plenum, New York, 1967), p. 26.